Production of J/Ψ on the nucleon and on deuteron targets

Jia-Jun Wu and T.-S. H. Lee
Physics Division, Argonne National Laboratory, Argonne, Illinois 60439, USA
(Received 21 March 2013; revised manuscript received 24 June 2013; published 17 July 2013)

A coupled-channel model with πN, ρN, and $J/\Psi N$ channels is developed to predict the $\pi + N \to J/\Psi + N$ cross sections. The J/Ψ-N interaction is parameterized in a form related to what has been predicted by the effective field theory approach and lattice QCD. The other interactions within the model are constrained by the decay width of $J/\Psi \to \rho + \pi$ and the total cross-sectional data of πN reactions. The calculated meson-baryon amplitudes are then used to predict the cross sections of the J/Ψ production on the deuteron target by including the contributions from the impulse term and the one-loop calculations of the final NN and $J/\Psi N$ rescattering effects. Predictions of the dependence of the cross sections of $\pi^- + p \to J/\Psi + n$, $\gamma + d \to J/\Psi + n + p$, and $\pi^+ d \to J/\Psi + p + p$ on the J/Ψ-N potentials are presented to examine the feasibility of experimental determinations of the J/Ψ-N interaction. Within the vector meson dominance model, we have also applied the constructed coupled-channel model to predict the $\gamma + p \to J/\Psi + p$ cross sections near the J/Ψ production threshold.

DOI: 10.1103/PhysRevC.88.015205 PACS number(s): 25.20.Lj, 24.85.+p, 13.75.Cs, 13.75.Gx

I. INTRODUCTION

The J/Ψ meson, as a $c\bar{c}$ bound state, can only interact with the nucleon through the gluon-exchange mechanism. By using the effective field theory method [1–4] and lattice QCD [5], it was found that the J/Ψ-N interaction is attractive. Strong attraction was also found [6] within a Pomeron-quark coupling model of $c\bar{c}$-nucleus interactions. Thus it is possible that J/Ψ and a system of nucleons can form nuclear bound states with *hidden charm*. If such *exotic* nuclear states indeed exist and can be detected, we can get useful information for understanding the role of gluons in nuclei.

The strengths of the J/Ψ-N interaction, parameterized as a Yukawa form $v_{J/\Psi N, J/\Psi N} = -\alpha \frac{e^{-\mu r}}{r}$ and deduced from Refs. [1–6], are rather different from each other. With $\mu = 0.60$ GeV, the calculated J/Ψ-N scattering lengths range from -0.05 fm using $\alpha = 0.06$ of Ref. [4] to -8.83 fm using $\alpha = 0.60$ of Ref. [6]. To understand quantitatively the role of gluons in hadron interactions, it is important to investigate how the J/Ψ-N interaction can be extracted from experiments to test these theoretical models. This is the objective of this work. Clearly, this is also a necessary step toward searching for possible nuclear bound states with hidden charm, as investigated in Ref. [7].

We first consider the $\pi + N \to J/\Psi + N$ reaction. At energies above the J/Ψ production threshold, this reaction is strongly influenced by many possible reaction channels, such as ρN, $\pi\pi N$, $\pi\pi\pi N$, $\pi\pi K\Lambda$ channels, because of the unitarity condition. To proceed, we cast this complex reaction problem into a manageable coupled-channel model with only πN, ρN, and $J/\Psi N$ channels. The interaction $v_{J/\Psi N, J/\Psi N}$ is chosen to be of a form related to the Yukawa form of Refs. [1–6]. With the J/Ψ-π-ρ coupling constant determined [7] by the partial decay width of $J/\Psi \to \pi\rho$, we can calculate the πN, $\rho N \to J/\Psi N$ transition potentials $v_{\rho N, J/\Psi N}$ and $v_{\pi N, J/\Psi N}$ by using the one-π and one-ρ exchange mechanisms, respectively, as illustrated in Fig. 1. The other interactions, which do not connect with the $J/\Psi N$ channel directly, will be treated as phenomenological complex potentials with their parameters constrained by reproducing the total cross sections of πN reactions and $\pi N \to \rho N$ reactions in the considered energy region. We also constrain these potentials by reproducing the total cross-sectional data of $\gamma p \to \rho^0 p$ which can be related qualitatively to $\rho^0 p \to \rho^0 p$ within the vector meson dominance model. To facilitate the experimental determination of the J/Ψ-N interaction, we present results showing the dependence of the calculated cross sections of $\pi^- + p \to J/\Psi + n$ on the potential $v_{J/\Psi N, J/\Psi N}$.

With the meson-baryon amplitudes generated from the constructed coupled-channel model described above and the Pomeron-exchange model of $\gamma + N \to J/\Psi + N$ we had developed in Ref. [7], we then examine the dependence of the $\gamma + d \to J/\Psi + p + n$ cross sections on $v_{J/\Psi N, J/\Psi N}$. We also follow the suggestion of Ref. [8] to investigate the $\pi^+ + d \to J/\Psi + p + p$ reaction. Instead of using the factorization approximation in Ref. [8], we have performed complete one-loop calculations to account for both the on- and off-shell $J/\Psi N$ final-state interactions. In addition, we also include the effects due to the final NN interaction by using the scattering T-matrix generated from the Bonn potential [9].

If we use the vector meson dominance hypothesis to convert the incoming photon into J/Ψ and ρ, we can predict the $\gamma + N \to J/\Psi + N$ cross sections within the constructed coupled-channel model. We see that our predictions also depend on the J/Ψ-N potential $v_{J/\Psi N, J/\Psi N}$. We also present these results, which could be tested in a forthcoming experiment [10].

In Sec. II, we present our coupled-channel model for J/Ψ production on the nucleon. The formula for calculating the meson-baryon reaction amplitudes are given in Sec. III. In Sec. IV, we give the formula for calculating the cross sections of the $\pi + N \to J/\Psi + N$ and $\gamma/\pi + d \to J/\Psi + N + N$ reactions. Our results are presented in Sec. V. A summary is given in Sec. VI.

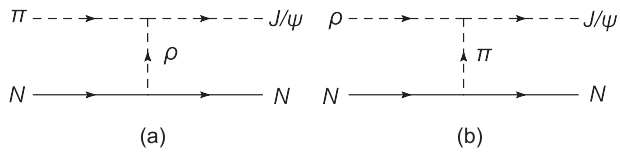

FIG. 1. Reaction mechanisms of $\pi + N \to J/\psi + N$ (left) and $\rho + N \to J/\psi + N$ (right).

II. COUPLED-CHANNEL MODEL FOR J/Ψ PRODUCTION

At energies near the J/Ψ production threshold, the πN reactions involve many meson-baryon channels such as $\pi\pi N$, $\pi\pi\pi N$, and $\pi\pi K\Lambda$. Within the formulation of Ref. [11], the scattering T matrix for such reactions are defined by the following coupled-channel equations:

$$T_{\alpha,\beta}(E) = v_{\alpha,\beta} + \sum_{\gamma} v_{\alpha,\gamma} G_{\gamma}(E) T_{\gamma,\beta}, \tag{1}$$

where α, β, γ denote the considered channels, $G_{\alpha}(E)$ is the meson-baryon propagator of channel α, and $v_{\alpha,\beta}$ are the interaction potentials.

For investigating the J/Ψ-N interaction, we treat πN and ρN channels explicitly since their interactions with the $J/\Psi N$ channel can be calculated, as is explained later. We thus set $\alpha, \beta, \gamma = J/\Psi N, \pi N, \rho N, X$ in Eq. (1), where X denotes collectively all other channels. By using the standard projection operator technique [11,12], we can cast Eq. (1) into

$$T_{i,j}(E) = V_{i,j}(E) + \sum_{k} V_{i,k}(E) G_k(E) T_{k,j}(E), \tag{2}$$

where $i, j, k = J/\Psi N, \pi N, \rho N$. The energy-dependent interactions in Eq. (2) are

$$V_{i,j}(E) = v_{i,j} + \sum_{X} v_{i,X} G_X(E)[1 + t_{X,X}(E) G_X(E)] v_{X,j}, \tag{3}$$

where the scattering amplitude $t_{X,X}$ in the subspace of the channel X is defined by

$$t_{X,X}(E) = v_{X,X} + v_{X,X} G_X(E) t_{X,X}(E). \tag{4}$$

We now turn to defining the interaction potentials v_{ij} in Eq. (3). As noticed in Refs. [3,7], the decay width $\Gamma_{J/\Psi,\rho\pi}$ of $J/\Psi \to \pi\rho$ is significant. From the value of $\Gamma_{J/\Psi,\rho\pi}$ listed by the Particle Data Group (PDG), we can determine [7] the coupling constant $g_{J/\Psi,\pi\rho}$ of the following interaction Lagrangian:

$$L_{J/\Psi\pi\rho} = -\frac{g_{J/\Psi,\pi\rho}}{m_{J/\Psi}} \epsilon^{\mu\nu\alpha\beta} \partial_{\mu} \rho_{\nu} \partial_{\alpha} \phi_{J/\Psi,\beta} \phi_{\pi}. \tag{5}$$

We find [7] $g_{J/\Psi,\pi\rho} = 0.032$. By using $L_{J/\Psi\pi\rho}$ and the well-known [13] Lagrangian $L_{\pi NN}$ and $L_{\rho NN}$, we can calculate one-π (one-ρ) exchange transition potential of the $\rho + N \to J/\Psi + N$ ($\pi + N \to J/\Psi + N$) process, as illustrated in Fig. 1. Explicitly, their matrix elements can be written (with the normalization to be specified in Sec. III and omitting spin and isospin indices) as

$$\begin{aligned}
&\langle \vec{p}_{J/\psi}, \vec{p}_{N_f} | v_{J/\psi N,\pi N} | \vec{p}_{\pi}, \vec{p}_{N_i} \rangle \\
&= \frac{1}{(2\pi)^3} \frac{1}{\sqrt{2E_{J/\Psi}(\vec{p}_{J/\psi})}} \sqrt{\frac{m_N}{E_N(\vec{p}_{N_f})}} \sqrt{\frac{m_N}{E_N(\vec{p}_{N_i})}} \\
&\times \frac{1}{\sqrt{2E_{\pi}(\vec{p}_{\pi})}} \left(-\frac{g_{J/\psi\rho\pi}}{m_{J/\psi}} g_{\rho NN} \right) \epsilon_{\mu\nu\alpha\beta} q^{\mu} p^{\alpha}_{J/\psi} \varepsilon^{\beta}(p_{J/\Psi}) \\
&\times \frac{1}{q^2 - m_{\rho}^2} \bar{u}_{\vec{p}_{N_f}} \left[\gamma^{\nu} - \frac{\not{q} q^{\nu}}{m_{\rho}^2} + \frac{\kappa_{\rho}}{4m_N} (\gamma^{\nu} \not{q} - \not{q} \gamma^{\nu}) \right] u_{\vec{p}_{N_i}},
\end{aligned} \tag{6}$$

$$\begin{aligned}
&\langle \vec{p}_{J/\psi}, \vec{p}_{N_f} | v_{J/\psi N,\rho N} | \vec{p}_{\rho}, \vec{p}_{N_i} \rangle \\
&= \frac{-1}{(2\pi)^3} \frac{1}{\sqrt{2E_{J/\Psi}(\vec{p}_{J/\psi})}} \sqrt{\frac{m_N}{E_N(\vec{p}_{N_f})}} \sqrt{\frac{m_N}{E_N(\vec{p}_{N_i})}} \frac{1}{\sqrt{2E_{\rho}(\vec{p}_{\rho})}} \\
&\times \left(\frac{g_{J/\psi\rho\pi}}{m_{J/\psi}} \frac{f_{\pi NN}}{m_{\pi}} \right) \epsilon_{\mu\nu\alpha\beta} p^{\mu}_{\rho} \varepsilon^{\nu}(p_{\rho}) p^{\alpha}_{J/\psi} \varepsilon^{\beta}(p_{J\Psi}) \\
&\times \frac{1}{q^2 - m_{\pi}^2} \bar{u}_{\vec{p}_{N_f}} \not{q} \gamma^5 u_{\vec{p}_{N_i}},
\end{aligned} \tag{7}$$

where $q = p_{N_i} - p_{N_f}$ and the coupling constants $g_{\rho NN} = 6.20$, $\kappa_{\rho} = 1.825$, $f_{\pi NN} = \sqrt{4\pi \times 0.80}$ are taken from a dynamical model [13] of πN scattering. All external particles of the matrix element of the above equations are on their mass shell with their momenta defined as $p_a = (E_a(\vec{p}_a), \vec{p}_a)$ and $E_a(\vec{p}_a) = [m_a^2 + \vec{p}_a^2]^{1/2}$.

We assume that the mesons and baryons in the channel X do not contain charmed quarks. The coupling between X and $J/\Psi N$ can then be neglected and we can set $v_{J/\Psi N,X} = 0$. It follows that for the interactions involving $J/\Psi N$, the second term of Eq. (3) vanishes and we have the following simplification:

$$V_{\pi N,J/\Psi N} = v_{\pi N,J/\Psi N}, \tag{8}$$

$$V_{\rho N,J/\Psi N} = v_{\rho N,J/\Psi N}, \tag{9}$$

$$V_{J/\Psi N,J/\Psi N} = v_{J/\Psi N,J/\Psi N}. \tag{10}$$

The matrix elements for $v_{\pi N,J/\Psi N}$ and $v_{\rho N,J/\Psi N}$ have been given in Eqs. (6) and (7). For $v_{J/\Psi N,J/\Psi N}$, we follow Refs. [2–5] and use the following Yukawa form:

$$v_{J/\Psi N,J/\Psi N}(r) = -\alpha \frac{e^{-\mu_0 r}}{r}. \tag{11}$$

To be consistent with the relativistic expressions in Eqs. (6) and (7), we assume that Eq. (11) is the nonrelativistic limit of a one-scalar meson exchange amplitude in field theory. We then obtain

$$\begin{aligned}
&\langle \vec{p}'_{J/\psi}, \vec{p}_{N_f} | v_{J/\Psi N,J/\Psi N} | \vec{p}_{J/\Psi}, \vec{p}_{N_i} \rangle \\
&= \frac{1}{(2\pi)^3} \frac{1}{\sqrt{2E_{J/\Psi}(\vec{p}'_{J/\psi})}} \sqrt{\frac{m_N}{E_N(\vec{p}_{N_f})}} \sqrt{\frac{m_N}{E_N(\vec{p}_{N_i})}} \\
&\times \frac{1}{\sqrt{2E_{J/\Psi}(\vec{p}_{J/\psi})}} [g_{\nu\mu} \varepsilon^{\nu}(p'_{J/\psi}) \varepsilon^{\mu}(p'_{J/\psi})] \\
&\times \frac{V_0}{q^2 - \mu_0^2} \bar{u}_{\vec{p}_{N_f}} u_{\vec{p}_{N_i}},
\end{aligned} \tag{12}$$

where $V_0 = -8\alpha\pi m_{J/\Psi}$, and $q = p_{N_i} - p_{N_f}$.

Since $v_{\pi N,X}$, $v_{\rho N,X}$, and $t_{XX}(E)$ cannot be calculated theoretically, we determine $V_{i,j}(E)$ with $i, j = \pi N, \rho N$ in Eq. (3) phenomenologically. For simplicity, we assume that they all have the following local form in the nonrelativistic limit:

$$V_{i,j}(E) = v^0_{i,j}(E) f_{i,j}(\vec{r}); \quad i, j = \pi N, \rho N, \tag{13}$$

where $f_{i,j}(\vec{r})$ is unitless such as $f_{i,j}(\vec{r}) = 1/(1 + e^{(r-r_0)/t})$ or e^{-r^2/b^2}. In the strong absorption (diffractive) model [12], the form of $f_{i,i}(\vec{r})$ for $i = 1, 2$ is similar to the nucleon density. We specify $f_{i,j}(\vec{r})$ later.

We next define

$$F_{i,j}(\vec{q}, E) = v^0_{i,j}(E) \int e^{-i\vec{q}\cdot\vec{r}} f_{i,j}(\vec{r}) d\vec{r}. \tag{14}$$

When including appropriate covariant spin factors, the matrix elements corresponding to the form of Eq. (13) are taken to be

$$\begin{aligned}
&\langle \vec{p}'_\pi, \vec{p}_{N_f} | V_{\pi N,\pi N}(E) | \vec{p}_\pi, \vec{p}_{N_i} \rangle \\
&\quad = \frac{1}{(2\pi)^3} \bar{u}_{\vec{p}_{N_f}} F_{\pi N,\pi N}(\vec{q}, E)\, u_{\vec{p}_{N_i}}, \qquad (15) \\
&\langle \vec{p}'_\rho, \vec{p}_{N_f} | V_{\rho N,\rho N}(E) | \vec{p}_\rho, \vec{p}_{N_i} \rangle \\
&\quad = \frac{1}{(2\pi)^3} \varepsilon^\nu_\rho(p'_\rho) \bar{u}_{\vec{p}_{N_f}} F_{\rho N,\rho N}(\vec{q}, E)\, u_{\vec{p}_{N_i}} \varepsilon_{\rho,\nu}(p_\rho), \qquad (16) \\
&\langle \vec{p}_\rho, \vec{p}_{N_f} | V_{\rho N,\pi N}(E) | \vec{p}_\pi, \vec{p}_{N_i} \rangle \\
&\quad = \frac{1}{(2\pi)^3} \frac{1}{m_\pi} p^\mu_\pi \varepsilon_\mu(p_\rho) F_{\rho N,\pi N}(\vec{q}, E)\, \bar{u}_{\vec{p}_{N_f}} \left[\frac{1}{m_\pi} \gamma_5 \not{q} \right] u_{\vec{p}_{N_i}}. \qquad (17)
\end{aligned}$$

We determine the parameters $v^0_{i,j}$ and $f_{i,j}(\vec{r})$ phenomenologically by fitting the total cross sections of πN and $\pi N \to \rho N$, and the $\gamma N \to \rho N$ cross sections which can be calculated from the predicted $\rho N \to \rho N$ amplitudes using the vector meson dominance hypothesis.

III. CALCULATIONS OF REACTION AMPLITUDES

In this work we follow the formulation of Ref. [11] within which the scattering T matrix is related to the S matrix by

$$S_{f,i}(E) = \delta_{f,i} - (2\pi) i \delta(E_f - E_i) \delta(\vec{P}_f - \vec{P}_i) T_{f,i}(E), \tag{18}$$

where E_α and $\vec{P}_\alpha$ are the total energy and momentum of the state α. The normalizations for the plane wave state $|\vec{k}\rangle$ and bound state $|\Phi_a\rangle$ are defined by

$$\langle \vec{k} | \vec{k}' \rangle = \delta(\vec{k} - \vec{k}'), \tag{19}$$

$$\langle \Phi_a | \Phi_b \rangle = \delta_{ab}. \tag{20}$$

A. Meson-baryon reaction amplitudes

In our calculations, we need the meson-baryon (MB) matrix elements in a fast moving frame. Following the instant form of relativistic quantum mechanics [14], we write for the two-particle $M(\vec{p}_M) + B(\vec{p}_B) \to M'(\vec{p}'_M) + B'(p'_B)$ transition

$$\begin{aligned}
&\langle \vec{p}'_M m'_{j_M}, m'_{i_M}; \vec{p}'_B m'_{j_B}, m_{\tau_B} | T_{M'B',MB}(E) | \vec{p}_M m_{j_M}, m_{i_M}; \vec{p}_B, m_{j_B} m_{\tau_B} \rangle \\
&\quad = J(\vec{P}, \vec{k}; \vec{p}_M, \vec{p}_B) J(\vec{P}', \vec{k}'; \vec{p}'_M, \vec{p}'_B) \langle m'_{j_M}, m'_{i_M}; m'_{j_B}, m'_{\tau_B} | t_{M'B',MB}(\vec{k}', \vec{k}; W) | m_{j_M}, m_{i_M}; m_{j_B}, m_{\tau_B} \rangle, \qquad (21)
\end{aligned}$$

where $[m_{j_M}, m_{i_M}]$ and $[m_{j_B}, m_{\tau_B}]$ are the z components of the spin-isospin quantum numbers for M and B, respectively. The total momenta $\vec{P}$, $\vec{P}'$ and the energy W in the center of mass system are

$$\vec{P} = \vec{p}_M + \vec{p}_B, \quad \vec{P}' = \vec{p}'_M + \vec{p}'_B, \quad W = [E^2 - \vec{P}^2]^{1/2}. \tag{22}$$

The relative momentum $\vec{k}$ and Jacobian $J(\vec{P}, \vec{k}; \vec{p}_M, \vec{p}_B)$ in Eq. (21) are defined by the Lorentz boost transformation [14]

$$\vec{k} = \vec{p}_M + \frac{\vec{P}}{M_0} \left[\frac{\vec{P} \cdot \vec{p}_M}{M_0 + H_0} - E_M(\vec{p}_M) \right], \tag{23}$$

$$J(\vec{P}, \vec{k}; \vec{p}_M, \vec{p}_B) = \left| \frac{\partial(\vec{P}, \vec{k})}{\partial(\vec{p}_M, \vec{p}_B)} \right|^{1/2} = \left[\frac{E_M(\vec{k}) E_B(\vec{k}) H_0}{E_M(\vec{p}_M) E_B(\vec{p}_B) M_0} \right]^{1/2}, \tag{24}$$

with

$$H_0 = E_M(\vec{p}_M) + E_B(\vec{p}_B), \tag{25}$$

$$\begin{aligned}
M_0 &= \sqrt{H_0^2 - \vec{P}^2} \\
&= E_M(\vec{k}) + E_B(\vec{k}). \qquad (26)
\end{aligned}$$

In Eq. (21), $t_{M'B',MB}(W)$ is the scattering operator in the center-of-mass frame. In the partial-wave representation, we can write

$$t_{M'B',MB}(\vec{k}', \vec{k}; W) = \sum_{J M_J, T M_T} \sum_{L'S', LS} |y^{J M_J, T M_T}_{L'S', M'B'}(\hat{k}')\rangle t^{JT}_{L'S', M'B', LS, MB}(k', k, W) \langle y^{J M_J, T M_T}_{LS, MB}(\hat{k})|, \tag{27}$$

where the angle-spin-isospin vector is defined by

$$|y^{JM_J,TM_T}_{LS,MB}(\hat{k})> = \sum_{m_{j_B}m_{j_M}} \sum_{m_{\tau_B}m_{i_M}} |m_{j_M}, m_{i_M}; m_{j_B}, m_{\tau_B}> \times \sum_{m_L,m_S} < J\ M_J|L\ S\ m_L\ m_S >< S\ m_s|j_M\ j_B\ m_{j_M}, m_{j_B} > \times < T\ M_T|i_M\ \tau_B\ m_{i_M}\ m_{\tau_B} > Y_{L\,m_L}(\hat{k}). \quad (28)$$

Here $[j_M, i_M]$ and $[j_B, \tau_B]$ are the spin-isospin quantum numbers for M and B, respectively; $\langle jm|j_1 j_2 m_1 m_2\rangle$ is the Clebsch-Gordon coefficient; and $Y_{Lm_L}(\hat{k})$ the spherical harmonic function, as defined in Ref. [15]. With the same partial-wave expansion, Eq. (28), for the meson-baryon potential $V_{i,j}(E)$, Eqs. (2) and (21) lead to the following coupled-channel equation:

$$t^{JT}_{L'S',M'B',LS,MB}(k', k.W) = V^{JT}_{L'S',M'B',LS,MB}(k', k.E) + \sum_{L''S'',M''B''} \int k''^2 dk'' V^{JT}_{L'S',M'B',L''S'',M''B''}(k', k''.E) G_{M''B''}(k'', W) t^{JT}_{L''S'',M''B'',LS,MB}(k', k.W), \quad (29)$$

where $MB, M'B', M''B'' = \pi N, \rho N, J/\Psi N$, and the propagator is

$$G_{MB}(k, W) = \frac{1}{W - E_M(k) - E_B(k) + i\epsilon}.$$

We use the procedures developed in Ref. [11] to calculate the potential matrix elements $V^{JT}_{L'S',M'B',L''S'',M''B''}(k', k''.E)$ from the matrix elements Eqs. (6)–(17).

B. Deuteron wave function and NN amplitude

For the calculations on the deuteron target, we need the deuteron bound state $|\Psi_{\vec{p}_d,M_{J_d}}\rangle$ moving with a high momentum $\vec{p}_d$. Following Ref. [14], it is defined by

$$\langle \vec{p}_1, m_{s_1}m_{\tau_1}; \vec{p}_2, m_{s_2}m_{\tau_2}|\Psi_{\vec{p}_d,M_d}\rangle = \delta(\vec{p}_d - \vec{p}_1 - \vec{p}_2)\langle \vec{p}_1, m_{s_1}m_{\tau_1}; \vec{p}_2, m_{s_2}m_{\tau_2}|\Phi_{\vec{p}_d,M_d}\rangle, \quad (30)$$

where

$$\langle \vec{p}_1, m_{s_1}m_{\tau_1}; \vec{p}_2, m_{s_2}m_{\tau_2}|\Phi_{\vec{p}_d,M_d}\rangle = J(\vec{p}_d, \vec{\kappa}; \vec{p}_1, \vec{p}_2)\langle m_{s_1}m_{\tau_1}; m_{s_2}m_{\tau_2}|\chi^{J_dM_d,T_dM_{T_d}}(\vec{\kappa})\rangle \quad (31)$$

with

$$|\chi^{J_dM_d,T_dM_{T_d}}(\vec{\kappa})\rangle = \sum_{l=0,2} |y^{J_dM_d,T_dM_{T_d}}_{ls_d,NN}(\hat{\kappa})\rangle u_l(\kappa). \quad (32)$$

Here $s_d = 1$ is the deuteron spin and $u_l(\kappa)$ is the usual deuteron radial wave function in its rest frame. The Jacobian $J(\vec{p}_d, \vec{\kappa}; \vec{p}_1, \vec{p}_2)$ and the relative momentum $\vec{\kappa}$ can be calculated by using the same Eqs. (23)–(26) with the replacement $\vec{k} \to \vec{\kappa}$, $\vec{p}_M \to \vec{p}_1$, $\vec{p}_B \to \vec{p}_2$, $\vec{P} \to \vec{p}_d$, and $MB \to NN$.

We also need the NN amplitude

$$\langle \vec{p}'_1 m'_{j_1}, m'_{\tau_1}; \vec{p}'_2 m'_{j_2}, m_{\tau_2}|T_{NN,NN}(E)|\vec{p}_1 m_{j_1}, m_{i_1}; \vec{p}_2, m_{j_2}m_{\tau_2}\rangle = J(\vec{P}, \vec{k}; \vec{p}_1, \vec{p}_2)J(\vec{P}', \vec{k}'; \vec{p}'_1, \vec{p}'_2)\langle m'_{j_1}, m'_{\tau_1}; m'_{j_2}, m'_{\tau_2}|t_{NN,NN}(\vec{k}', \vec{k}; W)|m_{j_1}, m_{\tau_1}; m_{j_2}, m_{\tau_2}\rangle. \quad (33)$$

The above matrix element can be calculated from Eqs. (21)–(28) with the replacement of $MB \to NN$. We generated the NN partial-wave matrix elements $t^{JT}_{L'S'NN,LSNN}(k', k; W)$ from the Bonn potential [9].

IV. CALCULATIONS OF CROSS SECTIONS

A. Cross sections of meson-baryon reactions

We need to evaluate the cross sections for the reactions involving three meson-baryon (MB) channels with $MB = \pi N, \rho N, J/\Psi N$. With the definitions Eqs. (18)–(21), the differential cross sections in the center of mass (c.m.) for the $M(\vec{k}) + B(-\vec{k}) \to M'(\vec{k}') + B'(-\vec{k}')$ reaction can be written as

$$\frac{d\sigma}{d\Omega} = \frac{(4\pi)^2}{k^2} \frac{\rho_{M'B'}(k')\rho_{MB}(k)}{(2j_M+1)(2j_B+1)} \sum_{m_{j_M},m_{j_B}} \sum_{m'_{j_M},m'_{j_B}} \left[\left|\langle m'_{j_M}, m'_{i_M}; m'_{j_B}, m'_{\tau_B}|t_{M'B',MB}(\vec{k}', \vec{k}; W)|m_{j_M}, m_{i_M}; m_{j_B}, m_{\tau_B}\rangle\right|^2\right], \quad (34)$$

where the matrix element of $t_{M'B',MB}(\vec{k}';W)$ can be calculated from Eqs. (27) and (28) and the solution of Eq. (29). The density of state is defined by

$$\rho_{MB}(k)=\pi\frac{kE_M(k)E_B(k)}{E}. \tag{35}$$

The total cross sections $\sigma^{el}_{\pi N,\pi N}$ of elastic $\pi N\to\pi N$ and $\sigma_{\pi N,\rho N}$ of $\pi N\to\rho N$ can be calculated using Eqs. (27) and (34), and the solution of the coupled-channel equation Eq. (29).

B. Total cross sections of πN reactions

The total cross sections $\sigma^{\rm tot}_{\pi N}$ can be obtained from the πN elastic scattering amplitude using the optical theorem. With our definitions Eqs. (18)–(21), we have

$$\sigma^{\rm tot}_{\pi N}=-{\rm Im}\,[\bar{f}_{\pi N,\pi N}(\theta=0)], \tag{36}$$

where the spin-averaged πN elastic scattering amplitude is

$$\bar{f}_{\pi N,\pi N}(\theta)=\frac{(4\pi)^2}{k^2}\frac{\rho_{\pi N}(E)}{2j_N+1}\left[\sum_{m_{j_N}}\left\langle 0,m_{i_\pi};m_{j_N},m_{\tau_N}\left|t_{\pi N,\pi N}(\vec{k}',\vec{k};E)\right|0,m_{i_\pi};m_{j_N},m_{\tau_N}\right\rangle\right] \tag{37}$$

and $k=|\vec{k}|=|\vec{k}'|$ is the on-shell momentum, and $\cos\theta=\hat{k}'\cdot\hat{k}$.

C. Cross sections of photoproduction of J/Ψ and ρ

We now note that with the vector meson dominance hypothesis, we can predict the cross section of $\gamma+p\to J/\Psi+p$ within the constructed coupled-channel model. This is done by writing the amplitude for $\gamma(\vec{q})+p(-\vec{q})\to J/\Psi(\vec{k}')+p(-\vec{k}')$ as

$$\begin{aligned}\left\langle m'_{J/\Psi},m'_{j_N}\left|t_{J/\Psi p,\gamma p}(\vec{k}',\vec{q};W)\right|\lambda_\gamma,m_{j_N}\right\rangle=&\sum_{m_{J/\Psi}}\left\langle m'_{J/\Psi},m'_{j_N}\left|t_{J/\Psi p,J/\Psi p}(\vec{k}',\vec{k};W)\right|m_{J/\Psi},m_{j_N}\right\rangle\frac{e}{f_{J/\Psi}}\delta_{m_{J/\Psi},\lambda_\gamma}\\&+\sum_{m_\rho}\left\langle m'_{J/\Psi},m'_{j_N}\left|t_{J/\Psi p,\rho^0 p}(\vec{k}',\vec{k};W)\right|m_{\rho^0},m_{j_N}\right\rangle\frac{e}{f_\rho}\delta_{m_{\rho^0},\lambda_\gamma},\end{aligned} \tag{38}$$

where $f_{J/\Psi}=11.2$ and $f_\rho=5.33$.

Obviously we can get the $\gamma(\vec{q})+p(-\vec{q})\to\rho^0(\vec{k}')+p(-\vec{k}')$ amplitude from Eq. (38) by interchanging J/Ψ and ρ^0. This will allow us to calculate the total cross section $\sigma_{\gamma p,\rho^0 p}$ of $\gamma p\to\rho^0 p$. Clearly, within this model based on the vector meson dominance hypothesis, $\sigma_{\gamma p,\rho^0 p}$ is closely related to the total cross section of $\rho^0 p\to\rho^0 p$, which cannot be obtained experimentally but can be essential in determining the parameters associated with our phenomenological potential $V_{\rho N,\rho N}(E)$.

D. Cross sections for $\gamma+d\to J/\Psi+n+p$

In Fig. 2, we illustrate the mechanisms included in our calculations of the cross sections of J/Ψ production on the deuteron target. Since we are mainly interested in the J/Ψ-N interaction [Fig. 2(c)], we examine how the predicted cross sections depend on the J/Ψ-N relative momentum in the final $J/\Psi+n+p$ state. This can be done most effectively by considering the following differential cross section in the c.m. frame of the $\gamma(\vec{q})+d(-\vec{q})\to J/\Psi(\vec{k})+n(\vec{p}_n)+p(\vec{p}_p)$ reaction,

$$\begin{aligned}\frac{d^2\sigma}{d\Omega_p d|\vec{\kappa}_{J/\psi}|}=&(2\pi)^4\frac{E_\gamma(\vec{q})E_d(\vec{q})}{|\vec{q}|W}\int d\Omega_{\hat{\vec{\kappa}}_{J/\psi}}\vec{\kappa}^2_{J/\psi}\frac{E_n(\vec{p}_n)E_{J/\psi}(\vec{k})E_p(\vec{p}_p)}{E_n(-\vec{\kappa}_{J/\psi})E_{J/\psi}(\vec{\kappa}_{J/\psi})}\frac{M_0|\vec{p}_p|}{W}\\&\times\frac{1}{2(2J_d+1)}\sum_{\lambda_\gamma,m_d}\sum_{m_{J/\psi},m_n,m_p}\left|\langle\vec{k}\,m_{J/\psi},\ \vec{p}_p\,m_p,\ \vec{p}_n\,m_n|\hat{T}^{\rm Imp}+\hat{T}^{J/\psi N}+\hat{T}^{NN}\left|\vec{q}\ \lambda_\gamma,\ \Phi_{-\vec{q}\,m_d}\right\rangle\right|^2,\end{aligned} \tag{39}$$

where $\vec{q}$ is the photon momentum chosen to be in the quantization z direction, $\Phi_{\vec{p}_d,m_d}$ is the deuteron with momentum $\vec{p}_d=-\vec{q}$, and $\vec{p}_n$, $\vec{p}_p$, and $\vec{k}$ are the momenta of the final proton, neutron, and J/ψ, respectively. $\vec{\kappa}_{J/\psi}=(|\vec{\kappa}_{J/\psi}|,\Omega_{\kappa_{J/\psi}})$

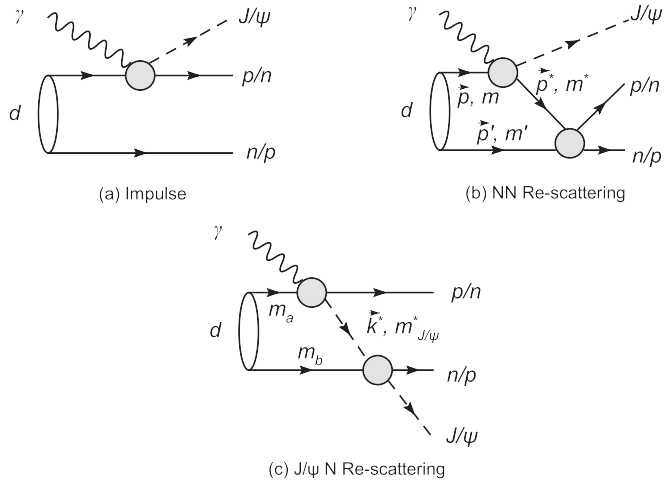

FIG. 2. Graphical representation of J/ψ photoproduction on the deuteron. Panels (a), (b), and (c) correspond, respectively, to the impulse contribution, Eq. (43); NN rescattering, Eq. (50); and $J/\psi N$ rescattering, Eq. (49).

is the momentum of J/Ψ in the c.m. of the J/Ψ-N subsystem. The amplitudes $\hat{T}^{\rm Imp}$, $\hat{T}^{NN}$, and $\hat{T}^{J/\Psi N}$ are calculated from the impulse (a), NN rescattering (b), and J/Ψ-N rescattering (c) mechanisms shown in Fig. 2.

In Eq. (39), W is the invariant mass of γd and $M_0 = E_{J/\Psi}(\vec{\kappa}_{J/\psi}) + E_n(\vec{\kappa}_{J/\psi})$ is the invariant mass of the J/ψ-N system. The magnitude of the outgoing proton momentum $\vec{p}_p$ can be calculated from M_0 and W by

$$|\vec{p}_p| = \frac{1}{2W}\left[\left(W^2 - m_p^2 - M_0^2\right)^2 - 4m_p^2 M_0^2\right]^{1/2}. \quad (40)$$

The direction of $\vec{p}_p$ is specified by Ω_p with respect to the incident photon momentum $\vec{q}$. The other variables $\vec{k}$ for the outgoing J/Ψ and $\vec{p}_n$ for the outgoing neutron in Eq. (39) can then be calculated from $\vec{\kappa}_{J/\psi}$ and $\vec{p}_p$ as follows:

$$\vec{k} = \vec{\kappa}_{J/\psi} + \frac{\vec{p}_p}{M_0}\left(\frac{\vec{p}_p \cdot \vec{\kappa}_{J/\psi}}{M_0 + W - E_p(\vec{p}_p)} - E_{J/\psi}(\vec{\kappa}_{J/\psi})\right), \quad (41)$$

$$\vec{p}_n = -\vec{\kappa}_{J/\psi} + \frac{\vec{p}_p}{M_0}\left(-\frac{\vec{p}_p \cdot \vec{\kappa}_{J/\psi}}{M_0 + W - E_p(\vec{p}_p)} - E_n(\vec{\kappa}_{J/\psi})\right). \quad (42)$$

With Eqs. (40)–(42), all kinematic variables for calculating the integrand of Eq. (39) are completely fixed for a given Ω_p and $\vec{\kappa}_{J/\psi}$. Our task is to explore at what Ω_p, the calculated differential cross section $\frac{d^2\sigma}{d\Omega_p d|\vec{\kappa}_{J/\psi}|}$ is most sensitive to the amplitude $\hat{T}^{J/\psi N}$ for the J/Ψ-N rescattering mechanism (c) of Fig. 2.

In the following three subsections, we give formulas for evaluating the matrix elements of $T^{\rm Imp}$, T^{NN}, and $T^{J/\Psi N}$. We have evaluated the Clebsch-Gordon coefficients associated with the isospin quantum numbers in Eq. (21) and thus all isospin indices are suppressed and the amplitudes are on specific charged states specified explicitly as n for neutron, p for proton, etc.

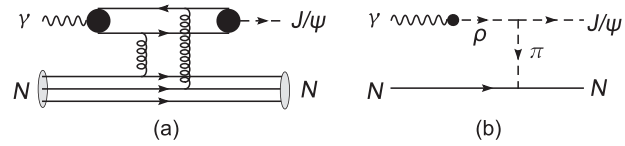

FIG. 3. Reaction mechanisms of $\gamma + N \to J/\psi + N$: (a) Pomeron exchange and (b) pion exchange.

1. Impulse amplitude

The impulse amplitude of Eq. (39) [Fig. 2(a)] can be straightforwardly written as

$$\begin{aligned}\langle \vec{k}\, m_{J/\psi},\ \vec{p}_p\, m_p,\ \vec{p}_n\, m_n|\hat{T}^{\rm Imp}|\vec{q}\ \lambda_\gamma,\ \Phi_{-\vec{q},m_d}\rangle \\ = \sum_{m_a}\big[\langle \vec{k}\, m_{J/\psi},\ \vec{p}_p\, m_p|T_{J/\psi p,\gamma p}|\vec{q}\ \lambda_\gamma,\ -\vec{q} - \vec{p}_n\, m_a\rangle \\ \times\langle -\vec{q} - \vec{p}_n\, m_a,\ \vec{p}_n\, m_n|\Phi_{-\vec{q}\, m_d}\rangle \\ + \langle \vec{k}\, m_{J/\psi},\ \vec{p}_n\, m_n|T_{J/\Psi n,\gamma n}|\vec{q}\ \lambda_\gamma,\ -\vec{q} - \vec{p}_p\, m_a\rangle \\ \times\langle \vec{p}_p\, m_p, -\vec{q} - \vec{p}_p\, m_a|\Phi_{-\vec{q}\, m_d}\rangle\big], \end{aligned} \quad (43)$$

where $\langle \vec{p}_p; m_p,\ \vec{p}_n; m_n|\Phi_{\vec{p}_d;m_d}\rangle$ has been defined by Eq. (31) (omitting isospin indices). The $\gamma + N_i \to J/\psi + N_f$ amplitudes in the above expression are taken from our previous work [7],

$$\begin{aligned}\langle \vec{k}\, m_{J/\Psi},\ \vec{p}_{N_f}\, m_{N_f}|T_{J/\Psi N,\gamma N}|\vec{q}\ \lambda_\gamma,\ \vec{p}_{N_i}\, m_{N_i}\rangle \\ = \frac{1}{(2\pi)^3}\frac{1}{\sqrt{2E_{J/\Psi}(\vec{k})}}\sqrt{\frac{m_N}{E_N(\vec{p}_{N_f})}}\sqrt{\frac{m_N}{E_N(\vec{p}_{N_i})}}\frac{1}{\sqrt{2|\vec{q}|}} \\ \times\big[\bar{u}_{m_{N_f}}(\vec{p}_{N_f})\epsilon^*_\mu(k, m_{J/\Psi})\big(\mathcal{M}^{\mu\nu}_{\mathbb{P}}(\vec{k}, \vec{p}_{N_f}, \vec{q}, \vec{p}_{N_i}) \\ + \mathcal{M}^{\mu\nu}_{\pi}(\vec{k}, \vec{p}_{N_f}, \vec{q}, \vec{p}_{N_i})\big)\epsilon_\nu(\vec{q}, \lambda_\gamma)u_{m_{N_i}}(\vec{p}_{N_i})\big] \end{aligned} \quad (44)$$

where $\mathcal{M}^{\mu\nu}_{\mathbb{P}}$ and $\mathcal{M}^{\mu\nu}_{\pi}$ are the contributions from the Pomeron exchange and π exchange mechanisms, respectively, as shown in Fig. 3.

For the Pomeron exchange, the amplitude can be written as

$$\mathcal{M}^{\mu\nu}_{\mathbb{P}}(k, p_{N_f}, q, p_{N_i}) = G_{\mathbb{P}}(s,t)\mathcal{T}^{\mu\nu}_{\mathbb{P}}(t,q), \quad (45)$$

with

$$G_{\mathbb{P}}(s,t) = \left(\frac{s}{s_0}\right)^{\alpha_P(t)-1}\exp\left\{-\frac{i\pi}{2}[\alpha_P(t) - 1]\right\}, \quad (46)$$

$$\begin{aligned}\mathcal{T}^{\mu\nu}_{\mathbb{P}}(t,q) = i12\sqrt{4\pi\alpha_{\rm em}}\frac{m^2_{J/\psi}\beta_c\beta_c}{f_{J/\psi}}\frac{1}{m^2_{J/\psi} - t} \\ \times\left(\frac{2\mu_0^2}{2\mu_0^2 + m^2_{J/\psi} - t}\right)F_1(t)\{\not{q}\, g^{\mu\nu} - q^\mu\gamma^\nu\}, \end{aligned} \quad (47)$$

where $t = (p_{N_i} - p_{N_f})^2$, $s = (q - p_{N_i})^2$, $\alpha_P(t) = \alpha_0 + \alpha'_P t$ with $\alpha_0 = 1.25$ and $\alpha'_P = 1/s_0 = 0.25\ {\rm GeV}^{-1}$, $\mu_0^2 = 1.1\ {\rm GeV}$, $\alpha_{\rm em} = e^2/4\pi = 1/\sqrt{137}$, $\beta_c = 0.84\ {\rm GeV}^{-1}$, $f_{J/\psi} = 11.2$, and $F_1(t) = (4M_N^2 - 2.8t)/(4M_N^2 - t)(1 - t/0.71\ ({\rm GeV}^2))^2$.

For the π exchange, the amplitude $\mathcal{M}_\pi^{\mu\nu}$ is

$$\mathcal{M}_\pi^{\mu\nu}(k, p_{N_f}, q, p_{N_i}) = \frac{e}{f_\rho}\frac{g_{J/\Psi,\rho^0\pi^0}}{m_{J/\Psi}}\frac{f_{\pi NN}}{m_\pi}\times\left(\frac{\Lambda^2}{\Lambda^2-t}\right)^4 \times\frac{1}{t-m_\pi^2}\epsilon^{\mu\nu\alpha\beta}k_\alpha q_\beta\left[\gamma\left(p_{N_f}-p_{N_i}\right)\right]\gamma^5, \quad (48)$$

where the $f_\rho = 5.33$, $g_{J/\Psi,\rho^0\pi^0} = 0.032$, and $\Lambda = 2000$ MeV.

All of the parameters specified above for evaluating Eqs. (46)–(48) were determined in Ref. [7] by fitting the total cross-sectional data of $\gamma + p \to J/\psi + p$ up to the invariant mass $W = 300$ GeV, as shown in Fig. 4.

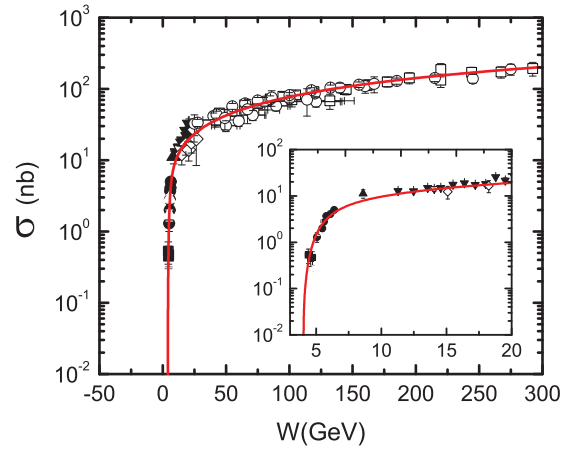

FIG. 4. (Color online) The total cross section of $\gamma + p \to J/\psi + p$. W is the invariant mass of the γp system. The red solid curves are calculated from the model of Ref. [7]. The data is from [16–24].

2. $J/\psi N$ rescattering amplitude

The amplitude $\hat{T}^{J/\psi N}$ in Eq. (39) [Fig. 2(c)] is

$$\langle \vec{k}\, m_{J/\psi},\ \vec{p}_p\, m_p,\ \vec{p}_n\, m_n|\hat{T}^{J/\psi N}|\vec{q}\ \lambda_\gamma,\ -\vec{q}\ m_d\rangle = \int d^3\vec{k}^* \sum_{m_a,\, m_b=-1/2,\, 1/2}\ \sum_{m^*_{J/\psi}=-1,0,1}\left\{\left[\frac{1}{W-E_N(\vec{p}_p)-E_{J/\psi}(\vec{k}^*)-E_N(-\vec{p}_p-\vec{k}^*)+i\epsilon}\right.\right.$$
$$\times\langle \vec{k}^*\, m^*_{J/\psi},\ \vec{p}_p\, m_p|T_{J/\psi p,\gamma p}|\vec{q}\ \lambda_\gamma,\ \vec{k}^*+\vec{p}_p-\vec{q}\ m_a\rangle\langle \vec{k}\, m_{J/\psi},\ \vec{p}_n\, m_n|T_{J/\psi n,J/\Psi n}(W_{J/\Psi n})|\vec{k}^*\, m^*_{J/\psi},\ \vec{k}+\vec{p}_n-\vec{k}^*\, m_b\rangle$$
$$\left.\left.\times\left\langle \vec{k}^*+\vec{p}_p-\vec{q}\ m_a,\ \vec{k}+\vec{p}_n-\vec{k}^*\, m_b\middle|\Phi_{-\vec{q}\ \lambda_d}\right\rangle\right]+[n\leftrightarrow p]\right\} \quad (49)$$

where $W_{J/\Psi n} = E_{J/\Psi}(p_{J/\Psi}) + E_N(p_n)$, $\langle \vec{p}\, m,\ \vec{p}',\ m'|\Phi_{\vec{p}_d;m_d}\rangle$ has been defined by Eq. (31), and $\langle \vec{k}\, m_{J/\psi},\ \vec{p}_n\, m_n|T_{J/\psi n,J/\Psi n}(W_{J/\Psi n})|\vec{k}^*\, m^*_{J/\psi},\ \vec{p}-\vec{k}^*\, m_b\rangle$ can be calculated using Eqs. (21)–(29). The first term in the bracket denotes the $\gamma + p \to J/\psi + p$ and $J/\psi + n \to J/\psi + n$, while the second term denotes $\gamma + n \to J/\psi + n$ and $J/\psi + p \to J/\psi + p$.

3. NN rescattering amplitude

The amplitude $\hat{T}^{NN}$ of Eq. (39) [Fig. 2(b)] can be written as

$$\langle \vec{k}\, m_{J/\psi},\ \vec{p}_p\, m_p,\ \vec{p}_n\, m_n|\hat{T}^{NN}|\vec{q}\ \lambda_\gamma,\ -\vec{q}\ m_d\rangle = \int d^3\vec{p}^*\frac{1}{W-E_{J/\psi}(\vec{k})-E_N(\vec{p}^*)-E_N(-\vec{k}-\vec{p}^*)+i\epsilon}$$
$$\times\sum_{m^*,m,m'=-1/2,1/2}\langle \vec{k}\, m_{J/\psi},\ \vec{p}^*m^*|T_{J/\Psi N,\gamma N}|\vec{q}\ \lambda_\gamma,\ \vec{p}\, m\rangle$$
$$\times\left[\langle \vec{p}_p\, m_p,\ \vec{p}_n\, m_n|T_{np,np}(E_{np})|\vec{p}^*\, m^*,\ \vec{p}'\, m'\rangle\right.$$
$$\left.\times\left\langle \vec{p}\, m,\ \vec{p}'\, m'\middle|\Phi_{-\vec{q}\, m_d}\right\rangle\right], \quad (50)$$

where $\vec{p}' = \vec{p}_p + \vec{p}_n - \vec{p}^*$, $\vec{p} = \vec{k} + \vec{p}^* - \vec{q}$, $E_{np} = E_N(p_p) + E_N(p_n)$, $\langle \vec{p}; m,\ \vec{p}'; m'|\Phi_{\vec{p}_d;m_d}\rangle$ has been defined by Eq. (31), and $\langle \vec{p}_p\, m_p,\ \vec{p}_n\, m_n|T_{np,np}(E_{np})|\vec{p}^*\, m^*,\ \vec{p}'\, m'\rangle$ can be calculated by using Eq. (33) and the $NN \to NN$ partial wave amplitudes generated from the Bonn potential [9].

E. Cross section of $\pi^+ + d \to J/\Psi + p + p$

By replacing $T_{J/\Psi N,\gamma N}$ by $T_{J/\Psi N,\pi N}$ and changing notations appropriately, the formula presented in Subsec. IVD can be used to calculate the differential cross section $\frac{d\sigma}{d\Omega_p d|\vec{k}_{J/\Psi}|}$ of $\pi^+ + d \to J/\Psi + p + p$.

V. RESULTS

Our first task is to determine the parameters of the potentials of the coupled-channel model presented in Sec. II. The parameters for the coupling potential $V_{i,J/\Psi N}$ with $i = \pi N, \rho N, J/\Psi N$ have been specified there. We determine the parameters of $V_{i,j} = v^0_{i,j}(E)f_{i,j}(r)$ with $i, j = \pi N, \rho N$, as already given in Eq. (13), by fitting the total cross-sectional data $\sigma^{\rm tot}_{\pi N}$ of the πN reaction, $\sigma^{el}_{\pi N,\pi N}$ of πN elastic scattering, $\sigma_{\pi N,\rho N}$ of $\pi N \to \rho N$, and $\sigma_{\gamma p,\rho^0 p}$ of $\gamma p \to \rho^0 p$. We achieve

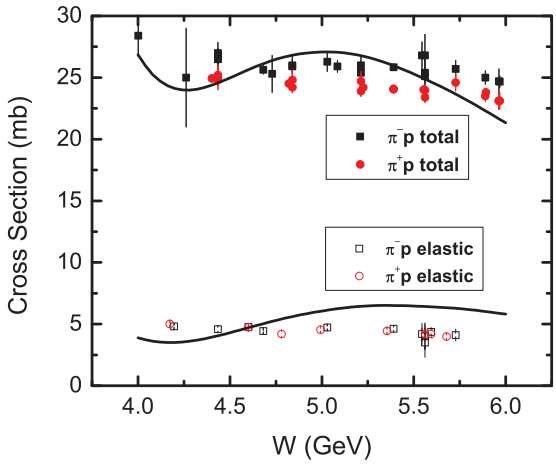

FIG. 5. (Color online) The fits to the data of the total cross sections $\sigma^{\rm tot}_{\pi^\pm p}$ of $\pi^\pm p$ reactions, and the total elastic $\pi^\pm p \to \pi^\pm p$ cross section $\sigma^{el}_{\pi^\pm p,\pi^\pm p}$. The data are from PDG [25].

this by choosing

$$f_{i,j}(r) = \frac{1}{1+e^{(r-c)/t}}, \tag{51}$$

where $c = 0.8$ fm, $t = 0.4$ fm for all $i, j = \pi N, \rho N$. The energy dependence of the total cross sections in the energy region near the J/Ψ production threshold (4 GeV $< W <$ 6 GeV) can be fitted qualitatively by setting

$$v^0_{i,j}(E) = (-i)\,[A + B(E - E_0)^2]. \tag{52}$$

Our fits to $\sigma^{\rm tot}_{\pi^\pm p}$ are shown in Fig. 5. The small isospin dependence in the data is neglected in our fits. In Fig. 6, we see that the fits to the total cross-sectional data of $\pi^\pm + p \to \rho^\pm + p$ (left) and $\gamma + p \to \rho^0 + p$ (right) are also reasonable. The resulting parameters A, B, and E_0 are listed in Table I.

Note that the forms Eqs. (51) and (52) are purely phenomenological, and our fits in Figs. 5 and 6 are only qualitatively. However, they are sufficient for estimating the order of magnitudes of the J/Ψ production cross sections. For a more quantitative calculation, we clearly need to improve this phenomenological aspect of our model.

TABLE I. The parameters for $v^0_{i,j}(E)$ of Eq. (52). E is the total energy in the enter of mass system.

i	j	A (GeV)	B (GeV^{-1})	E_0 (GeV)
πN	πN	0.43	1.18	4.0
πN	ρN	0.04	0.09	4.0
ρN	ρN	0.45	0.45	4.0

With the fits shown in Figs. 5 and 6, all of the parameters for our calculations are completely fixed. In the next few subsections, we present our predictions for future experimental determinations of the J/Ψ-N interaction.

A. $\pi^- + p \to J/\Psi + n$

The simplest experiment to determine the J/Ψ-N interaction within our coupled-channel model is to measure the cross sections of the $\pi^- + p \to J/\Psi + n$ reaction. We first observe that the coupled-channel effects can drastically change the magnitudes and the energy dependence of the predicted cross sections. This is illustrated in the left side of Fig. 7. In the absence of coupled-channel effects, the results from the Born approximation (setting $T_{J/\Psi N,\pi N} = V_{J/\Psi N,\pi N}$) are shown by the dotted curve. When the interactions associated with the $J/\Psi N$ channel, $V_{i,J/\Psi}$ with $i = \pi N, \rho N, J/\Psi N$, are included in solving the coupled-channel equation, we obtain the dashed curve, which is suppressed at high W in contrast to the raising behavior of the dotted curve from the Born approximation. When the complex potentials $V_{i,j}$ with $i, j = \pi N, \rho N$ are also included in our full calculations, we obtain the solid black curve. We see that these complex potentials can drastically reduce the magnitudes of the cross sections. This is due to the fact that most of the incident pions are absorbed before the J/Ψ production takes place. Within our model, this absorption effect is due to the very large imaginary part of $V_{\pi N,\pi N}$.

The coupled-channel effects on $J/\Psi + p \to J/\Psi + p$ are shown in the right side of Fig. 7. We note that the J/Ψ-N interaction, as defined in Eq. (11), is real and therefore does not have strong absorption effects on J/Ψ-N scattering.

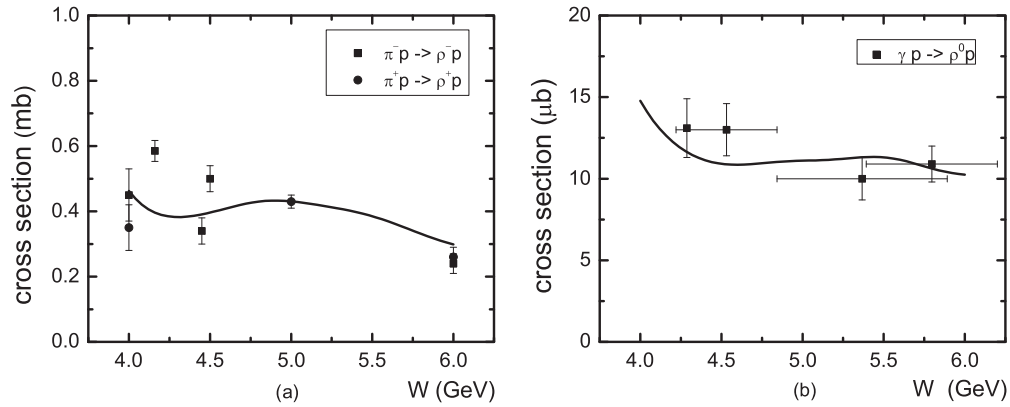

FIG. 6. The fits to the data of the total cross sections $\sigma_{\pi^\pm p\to\rho^\pm p}$ of $\pi^\pm p \to \rho^\pm p$ (left) and $\sigma_{\gamma p\to\rho^0 p}$ for $\gamma p \to \rho^0 p$ (right). The data of $\sigma_{\pi^\pm p\to\rho^\pm p}$ are from Ref. [26], and the data of $\sigma_{\gamma p\to\rho^0 p}$ are from Refs. [27–29].

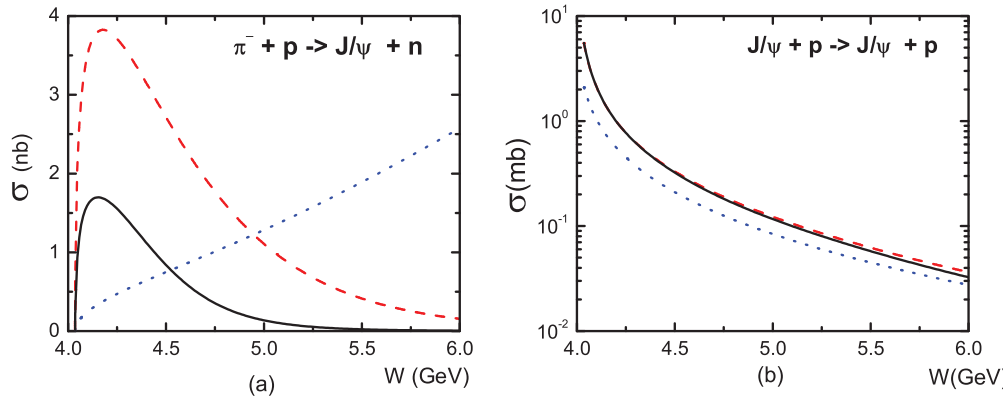

FIG. 7. (Color online) The cross sections of $\pi^- + p \to J/\Psi + n$ (left) and $J/\Psi + p \to J/\Psi + p$ (right). Black solid, full calculation; dashed (red online), coupled channel, but setting $V_{i,J/\Psi} = 0$ for $i, j = \pi N, \rho N$; and dotted (blue online), Born calculation $T_{i,j} = V_{i,j}$. W is the total energy in the c.m. frame.

By comparing the differences between the dotted curve of the Born approximation ($T_{J/\Psi N, J/\Psi N} = V_{J/\Psi N, J/\Psi N}$) and the dashed curve, we see that the coupled-channel effects due to $V_{i,J/\Psi}$ with $i = \pi N, \rho N, J/\Psi N$ is to increase the cross section at all W. The coupled-channel effects due to $V_{i,j}$ with $i, j = \pi N, \rho N$ are very small, as can be seen by comparing the dashed curve and the black solid curve in the right side of Fig. 7. This is due to the fact that the J/Ψ-π-ρ coupling constant $g_{J/\Psi\rho\pi} = 0.032$, calculated from the partial decay width of $J/\Psi \to \pi\rho$, is very small in the calculation of Eqs. (6) and (7) for the one-meson-exchange matrix elements of $v_{\rho N, J/\Psi}$ and $v_{\pi N, J/\Psi}$.

We next examine the dependence of the $\pi^- + p \to J/\Psi + n$ cross sections on the strength α of the J/Ψ-N potential $v_{J/\Psi N, J/\Psi N}$. The results from using $\alpha = 0.2, 0.09, 0.06$ are compared in the left side of Fig. 8. The predicted total cross sections at peak positions are about 1.5 nb. Such small cross sections are due to the strong absorption of the incident pion and that the $\pi N \to J/\Psi N$ transition potential $V_{\pi N, J/\Psi N}$ is weak, as discussed above. The differences between three results are significant only in the region near $W \sim 4.25$ GeV. On the other hand, the predicted $J/\Psi N \to J/\Psi N$ cross sections are more sensitive to α, as seen in the right side of Fig. 8. This suggests that J/Ψ-N interaction can be more easily determined in the reactions of J/Ψ production on the deuteron target in the kinematic region where the cross sections are sensitive to the $J/\Psi N \to J/\Psi N$ rescattering mechanism [Fig. 2(c)]. This is what we examine in the next two subsections.

B. $\gamma + d \to J/\Psi + n + p$

We consider only the energy region close to the J/Ψ production threshold. The results presented below and in the next subsection are calculated at the energy 100 MeV above the J/Ψ production.

As discussed in Sec. IV D, our main task is to use Eq. (39) to examine the dependence of the differential cross section $\frac{d\sigma}{d\Omega_p d|\vec{\kappa}_{J/\Psi}|}$ of this process on the J/Ψ-N potential $V_{J/\Psi N, J\Psi N}$. Obviously, we need to identify the region of the outgoing proton angle θ_p with respect to the incident photon where the J/Ψ-N rescattering mechanism [Fig. 2(c)] dominates. We find that this is in the region close to $\theta_p = 0$, as can be seen in the left side of Fig. 9. We see that in the low J/Ψ momentum,

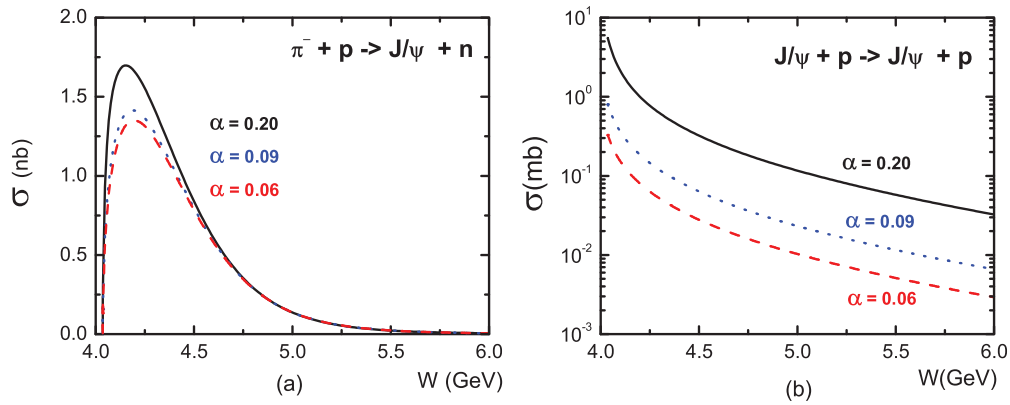

FIG. 8. (Color online) The total cross sections of $\pi^- + p \to J/\Psi + n$ (left) and $J/\psi + p \to J/\Psi + p$ (right). W is the total energy in the c.m. frame. The solid, dotted, and dashed curves are calculated by using the J/Ψ-N potential, Eq. (11), with $\mu = 0.6$ GeV and $\alpha = 0.20, 0.09, 0.06$, respectively.

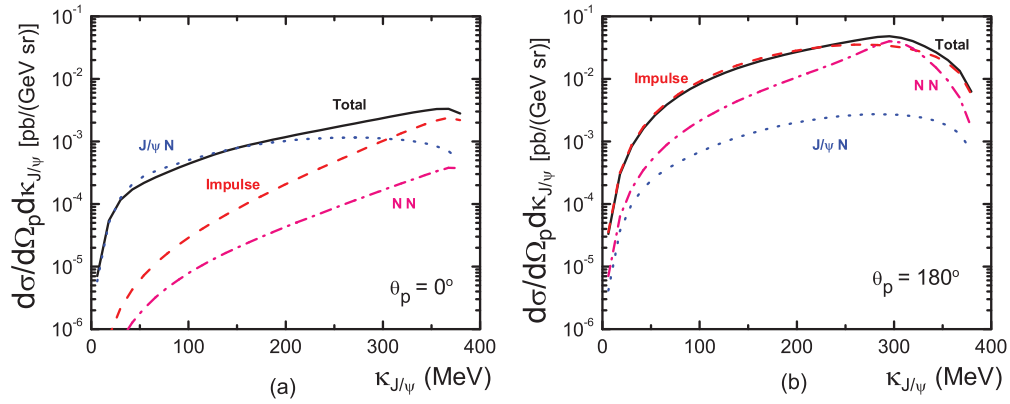

FIG. 9. (Color online) The differential cross section $d\sigma/(d\Omega_p d\kappa_{J/\Psi})$ of $\gamma + d \to J/\Psi + p + n$ vs the momentum $\kappa_{J/\Psi}$ of J/Ψ in the c.m. frame of the $J/\Psi + n$ subsystem. The results are from coupled-channel calculations using the J/Ψ-N potential, Eq. (11), with $\mu = 0.6$ GeV and $\alpha = 0.20$. θ_p in panels (a) and (b) are the angles between the incoming photon and the outgoing proton. The dashed (red online), dotted (blue online), and dashed-dotted (pink online) lines are the contributions from the amplitudes of the impulse term, $J/\Psi N$ rescattering, and NN rescattering, respectively. The black solid lines are the coherent sum of these three amplitudes.

$\kappa_{J/\Psi} <$ about 200 MeV, the contribution from the J/Ψ rescattering term (dotted curve) is much larger than that from the other two mechanisms. On the other hand, the impulse term dominates at $\theta_p = 180^\circ$ as seen in the right side of Fig. 9. Accordingly, three J/Ψ-N potentials with the strengths $\alpha = 0.2$, 0.09, and 0.06 obtained by the effective field theory approach and LQCD can be easily tested at $\theta_p = 0$, but less possible at $\theta_p = 180^\circ$. This is shown in Fig. 10.

We note that the J/Ψ-N scattering length can be related unambiguously to the cross section only in the energy region where the kinetic energy of the outgoing J/Ψ-N system is very low. To provide information for examining the feasibility of possible experimental determinations of this interesting quantity, we present the angular distribution of $\frac{d\sigma}{d\Omega_p d|\vec{\kappa}_{J/\Psi}|}$ at J/Ψ-n kinetic energy $T_{J/\Psi\text{-}n} = 30$ MeV (the relative J/Ψ-n momentum is $\kappa_{J/\Psi} = 200$ MeV) in Fig. 11. Our results are qualitatively similar to Fig. 12(a) of a recent investigation [30] of electroproduction of J/Ψ on the deuteron (note that their scattering angle $\theta_{\text{c.m.}}$ is the angle between the outgoing proton and the initial deuteron momentum, while our θ_p is the angle between the outgoing proton and the initial photon. Thus one needs to set $\theta_p = \pi - \theta_{\text{c.m.}}$ in comparing two results.) While the models and the considered kinematics are different, both investigations predict very small cross sections, which pose a serious challenge in extracting the J/Ψ-N scattering length model independently.

C. $\pi^+ + d \to J/\Psi + p + p$

For the calculated $\frac{d\sigma}{d\Omega_p d|\vec{\kappa}_{J/\Psi}|}$ of the $\pi^+ d \to J/\Psi + p + p$ reaction, we find that the impulse term dominates at all angles. Furthermore, the contributions from the J/Ψ-N rescattering [Fig. 2(c)] are weaker than those of the NN rescattering [Fig. 2(b)]. Nevertheless, the data from experiments on this reaction can be useful to determine the J/Ψ-N interaction. This is illustrated in Fig. 12 where the results from $\alpha = 0.20$, 0.09, and 0.06 for $\theta_p = 0$ and 180° are compared.

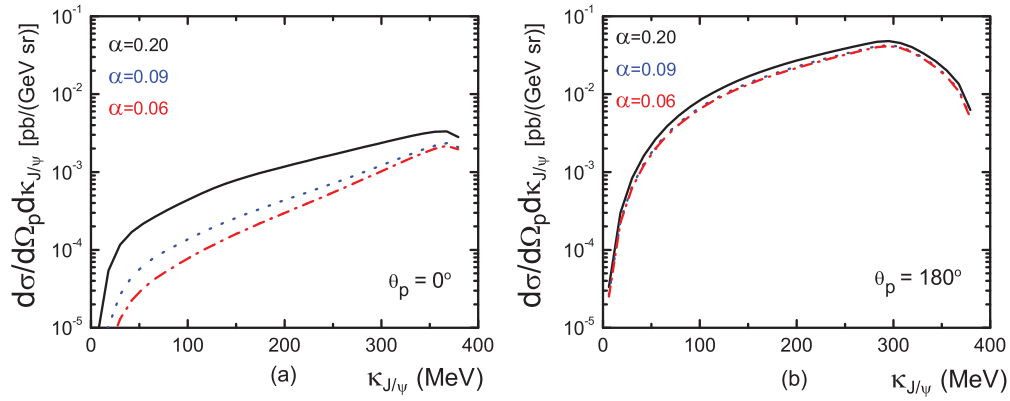

FIG. 10. (Color online) The differential cross section $d\sigma/(d\Omega_p d\kappa_{J/\Psi})$ of $\gamma + d \to J/\Psi + p + n$ vs the momentum $\kappa_{J/\Psi}$ of J/Ψ in the c.m. frame of the $J/\Psi + n$ subsystem. θ_p is the angle between the incoming photon and the outgoing proton. The solid, dotted (blue online), and dashed-dotted (red online) lines are from the coupled-channel calculations using the $J/\Psi N \to J/\Psi N$ potential, Eq. (11), with $\mu = 0.6$ GeV and $\alpha = 0.20$, 0.09, 0.06, respectively.

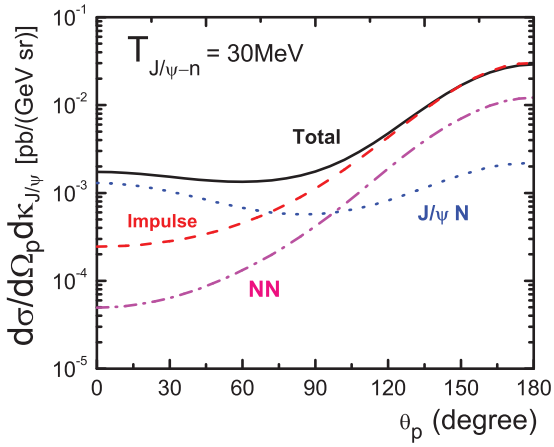

FIG. 11. (Color online) The differential cross section $d\sigma/(d\Omega_p d\kappa_{J/\psi})$ of $\gamma + d \to J/\Psi + p + n$ vs the angle θ_p between outgoing proton and incoming photon. The results are from coupled-channel calculations using the J/Ψ-N potential, Eq. (11), with $\mu = 0.6$ GeV and $\alpha = 0.20$. $T_{J/\psi\text{-}n}$ is kinematic energy of J/ψ-n system. The sets of lines are the same as in Fig. 9.

D. $\gamma p \to J/\Psi p$ in the coupled-channel model

With the vector meson dominance hypothesis, we can predict the cross section of $\gamma + p \to J/\Psi + p$ within the constructed coupled-channel model. This is done by using the amplitude given in Eq. (38). For three coupled-channel amplitudes calculated with $\alpha = 0.2$, 0.09, and 0.06 for $V_{J/\Psi N, J/\Psi N}$, our results are compared with those of the Pomeron-exchange model (dot-dashed curve, green online) in the left of Fig. 13.

We note that the coupled-channel model results are expected to be valid only at energies near J/Ψ production threshold where the data are rather uncertain. On the other hand, the use of Pomeron-exchange model at very low energies is also questionable. Our results for $\alpha = 0.06$ are close to the three data points near 4.5 GeV. At $W >$ about 5 GeV, we clearly need to improve the model. The data from the forthcoming experiment [10] at Jefferson Laboratory will be useful to clarify the situation.

In the right side of Fig. 13, we show that the coupled-channel effects can increase the cross section significantly. Our results here as well as those shown in Fig. 7 suggest that any attempt to determine the J/Ψ-N interaction must include the coupled-channel effects, as required by the unitarity condition.

VI. SUMMARY

We have developed a coupled-channel model with πN, ρN, and $J/\Psi N$ channels to predict the J/Ψ production on the nucleon. The J/Ψ-N interaction potential $V_{J/\Psi N, J/\Psi N}$ is taken from the calculations using the effective field theory method and lattice QCD. The $J/\Psi N \to \pi N, \rho N$ transition potentials $V_{J/\Psi N, \pi N}$ and $V_{J/\Psi N, \rho N}$ are calculated from one-ρ-exchange and one-π-exchange mechanisms with the parameters determined by the decay width of $J/\Psi \to \pi\rho$ and the previously determined πNN and ρNN coupling constants. The interactions $V_{i,j}$ with $i, j = \pi N, \rho N$ are treated as phenomenological complex potentials with their parameters constrained by the fits to the data of total cross sections of the πN reactions, $\pi N \to \pi N$, $\pi N \to \rho N$, and $\gamma p \to \rho^0 p$.

The calculated meson-baryon amplitudes are then used to predict the cross sections of $\gamma + d \to J/\Psi + N + N$ and $\pi + d \to J/\Psi + N + N$ reactions. The calculations on the deuteron target involve the contributions from the impulse term and the final NN and $J/\Psi N$ scattering. We have identified the kinematic region where the J/Ψ-N potentials can be distinguished in $\pi^- + p \to J/\Psi + n$, $\gamma + d \to J/\Psi + n + p$ and $\pi^+ + d \to J/\Psi + p + p$ reactions. Predictions of the dependence of the cross sections of these reactions on the J/Ψ-N potentials are presented. Our results shown in Figs. 8, 10, and 12 can be used to examine the feasibility of the experimental determinations of J/Ψ-N interactions.

Within the vector meson dominance model, we have also applied the constructed coupled-channel model to predict the $\gamma + p \to J/\Psi + p$ cross sections. Our results near the J/Ψ production threshold, as shown in Fig. 13, are very different from what can be calculated from the conventional Pomeron-exchange model, which is mainly constrained by

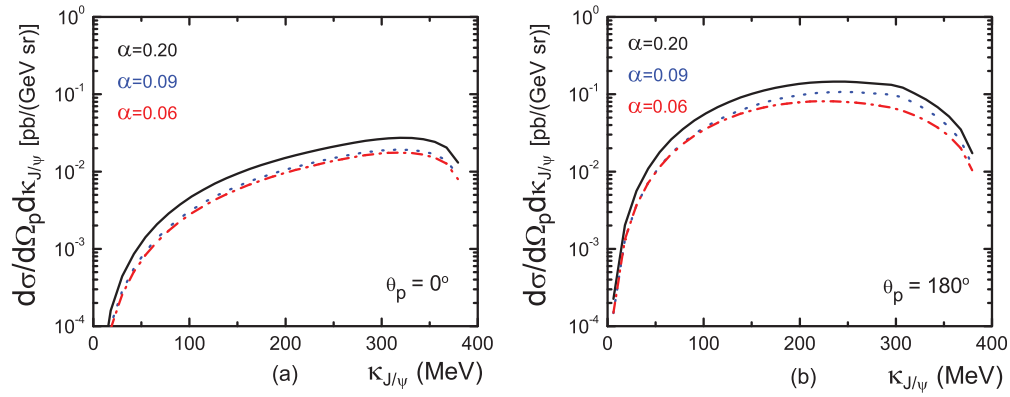

FIG. 12. (Color online) The differential cross section $d\sigma/(d\Omega_p d\kappa_{J/\Psi})$ of $\pi^+ + d \to J/\Psi + p + p$ vs the momentum $\kappa_{J/\Psi}$ of J/Ψ in the c.m. frame of the $J/\Psi + p$ subsystem. The black solid, dotted (blue online), and dashed-dotted (red online) lines are from the coupled-channel calculations using the J/Ψ-N potential, Eq. (11), with $\mu = 0.6$ GeV and $\alpha = 0.20$, 0.09, 0.06. θ_p is the angle between the incoming pion and the outgoing proton.

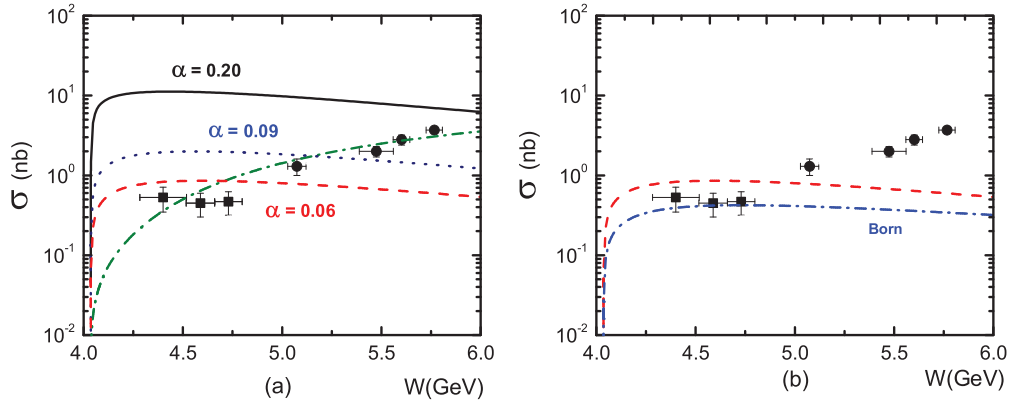

FIG. 13. (Color online) The cross section of $\gamma + N \to J/\Psi + N$ reaction. W is the total energy in the c.m. frame. In the left side, the black solid, dotted (blue online), dashed (red online) lines are calculated by using coupled-channel model with $\mu = 0.6$ GeV and $\alpha = 0.20, 0.09, 0.06$ and the dashed-dotted (green online) line is from Pomeron exchange. On the right side, the dashed (red online) and dashed-dotted (blue online) lines are from the full calculation and the Born approximation calculation $T_{i,j} = V_{i,j}$. The parameters of $v_{J/\Psi N, J/\Psi N}$ of the coupled-channel model are $\mu = 0.6$ GeV and $\alpha = 0.06$. The data are from Refs. [16–18].

the $\gamma p \to J/\Psi + p$ cross section at high energies. It will be interesting to distinguish these two models in the forthcoming experiment at Jefferson Laboratory [10].

ACKNOWLEDGMENTS

We thank R. Machleidt for providing us with the code for generating the NN amplitudes from the Bonn potential. This work is supported by the US Department of Energy, Office of Nuclear Physics Division, under Contract No. DE-AC02-06CH11357. This research used resources of the National Energy Research Scientific Computing Center, which is supported by the Office of Science of the US Department of Energy under Contract No. DE-AC02-05CH11231, and resources provided on "Fusion," a 320-node computing cluster operated by the Laboratory Computing Resource Center at Argonne National Laboratory.

[1] M. E. Peskin, Nucl. Phys. B **156**, 365 (1979).
[2] M. E. Luke, A. V. Manohar, and M. J. Savage, Phys. Lett. B **288**, 355 (1992).
[3] S. J. Brodsky and G. A. Miller, Phys. Lett. B **412**, 125 (1997).
[4] A. B. Kaidalov and P. E. Volkovitsky, Phys. Rev. Lett. **69**, 3155 (1992).
[5] T. Kawanai and S. Sasaki, Phys. Rev. D **82**, 091501 (2010).
[6] S. J. Brodsky, I. A. Schmidt, and G. F. de Teramond, Phys. Rev. Lett. **64**, 1011 (1990).
[7] J.-J. Wu and T.-S. H. Lee, Phys. Rev. C **86**, 065203 (2012).
[8] S. J. Brodsky, E. Chudakov, P. Hoyer, and J. M. Laget, Phys. Lett. B **498**, 23 (2001).
[9] R. Machleidt, Adv. Nucl. Phys. **19**, 189 (1989).
[10] Z.-E. Meziani, K. Hafidi, X. Qian, N. Sparveris *et al.*, PR12-12-006 (2012), PAC39, Jefferson Laboratory, 2012 (unpublished).
[11] A. Matsuyama, T. Sato, and T.-S. H. Lee, Phys. Rep. **439**, 193 (2007).
[12] Herman Feshbach, *Theoretical Nuclear Physics, Nuclear Reactions* (Wiley, New York, 1992).
[13] T. Sato and T.-S. H. Lee, Phys. Rev. C **54**, 2660 (1996).
[14] B. D. Keister and W. N. Polyzou, Adv. Nucl. Phys. **20**, 225 (1991).
[15] D. M. Brink and G. R. Satchler, *Angular Momentum* (Oxford University Press, Oxford, 1968).
[16] U. Camerini, J. G. Learned, R. Prepost, C. M. Spencer, D. E. Wiser, W. Ash, R. L. Anderson, D. Ritson *et al.*, Phys. Rev. Lett. **35**, 483 (1975).
[17] B. Gittelman, K. M. Hanson, D. Larson, E. Loh, A. Silverman, and G. Theodosiou, Phys. Rev. Lett. **35**, 1616 (1975).
[18] R. L. Anderson, SLAC-PUB-1471 (unpublished).
[19] M. E. Binkley, C. Bohler, J. Butler, J. P. Cumalat, I. Gaines, M. Gormley, D. Harding, R. L. Loveless *et al.*, Phys. Rev. Lett. **48**, 73 (1982).
[20] B. H. Denby, V. K. Bharadwaj, D. J. Summers, A. M. Eisner, R. G. Kennett, A. Lu, R. J. Morrison, M. S. Witherell *et al.*, Phys. Rev. Lett. **52**, 795 (1984).
[21] R. Barate *et al.* (NA14 Collaboration), Z. Phys. C **33**, 505 (1987).
[22] P. L. Frabetti *et al.* (E687 Collaboration), Phys. Lett. B **316**, 197 (1993).
[23] S. Aid *et al.* (H1 Collaboration), Nucl. Phys. B **472**, 3 (1996); A. Aktas *et al.* (H1 Collaboration), Eur. Phys. J. C **46**, 585 (2006).
[24] J. Breitweg *et al.* (ZEUS Collaboration), Z. Phys. C **76**, 599 (1997); S. Chekanov *et al.* (ZEUS Collaboration), Eur. Phys. J. C **24**, 345 (2002); Nucl. Phys. B **695**, 3 (2004); M. Derrick *et al.* (ZEUS Collaboration), Phys. Lett. B **350**, 120 (1995).
[25] J. Beringer *et al.* (Particle Data Group Collaboration), Phys. Rev. D **86**, 010001 (2012).
[26] A. Baldini, V. Flamino, W. G. Moorhead, D. R. O. Morrison, and Landolt-Börnstein, in *Numerical Data*

and Functional Relationships in Science and Technology, Total Cross Sections for Reactions of High Energy Particles, Vol. 12, edited by H. Schopper (Springer-Verlag, Berlin, 1988).

[27] Y. A. Aleksandrov, S. S. Baranov, A. S. Belousov, N. P. Budanov, Y. A. Vazdik, B. B. Govorkov, V. V. Kim, V. A. Kozlov *et al.*, Yad. Fiz. **32**, 651 (1980).

[28] J. Ballam, G. B. Chadwick, Y. Eisenberg, E. Kogan, K. C. Moffeit, P. Seyboth, I. O. Skillicorn, H. Spitzer *et al.*, Phys. Rev. D **7**, 3150 (1973).

[29] J. Park, M. Davier, I. Derado, D. E. C. Fries, F. F. Liu, R. F. Mozley, A. Odian, W. P. Swanson *et al.*, Nucl. Phys. B **36**, 404 (1972).

[30] G. T. Howell and G. A. Miller, Phys. Rev. C **88**, 015204 (2013).